SSRG International Journal of Electrical and Electronics Engineering
ISSN: 2348-8379/ https://doi.org/10.14445/23488379/IJEEE-V13I10P103

Volume 13 Issue 10, 25-36, October 2026
© 2026 Seventh Sense Research Group®

Original Article

A Gaussian Process Regression based MPPT Strategy for Interharmonic Mitigation in On-Grid PV Systems

Rakhee Rajagopal[1*,2], Latha Padinjaredath Govindan[1]

[1]*School of Engineering, Cochin University of Science and Technology, Ernakulam, Kerala, India.*
[2]*Department of Electrical and Electronics Engineering, Federal Institute of Science and Technology, Angamaly, Kerala, India.*

[1*]*Corresponding Author : rakheerajesh@cusat.ac.in*

Received: 22 May 2026 Revised: 27 August 2026 Accepted: 21 September 2026 Published: 28 October 2026

Abstract - *The widespread adoption of Photovoltaic (PV) systems as a renewable solution to rising energy demands has led to growing concerns regarding Power Quality (PQ) issues in grid current. The inherent intermittency of PV systems, along with several control techniques employed, is responsible for the generation of interharmonics that have severe impacts on the power system, including resonance and control instability. The severity of these issues increases with higher levels of PV penetration. Among the various contributing factors, the perturbation employed in the Maximum Power Point Tracking (MPPT) strategy for PV systems is reported as a significant source of interharmonics, especially under low power conditions. This paper investigates the influence of perturbation step size on MPPT performance and interharmonic emission in a 100-kW grid-connected PV system. The limitations of fixed and hybrid Perturb and Observe (P&O) methods are analyzed in terms of tracking speed and power quality indices. To overcome the limitations of conventional perturbation-based MPPT methods, a Gaussian Process Regression (GPR) based MPPT approach is presented in this paper. Comparative analysis in simulation demonstrates that the proposed GPR-based MPPT significantly reduces Total Harmonic Distortion (THD) as well as Total Interharmonic Distortion (TIHD) in the grid current, while achieving faster tracking speed, zero overshoot, and improved steady-state efficiency. The proposed method offers an effective solution for improving energy harvesting as well as power quality in grid-connected PV systems, especially under low-power operating conditions.*

Keywords - *MPPT, Interharmonics, Gaussian Process Regression, Power Quality, Grid-Connected PV system.*

1. Introduction

The rising energy needs due to population growth, as well as the exhaustion of fossil fuel resources and their environmental impacts, necessitate the need for sustainable energy alternatives like solar, wind and hydro power. Photovoltaic (PV) systems are one of the most reliable and widely adopted renewable energy technologies due to their scalability and life span (Z.Sandi 2024). Due to the various policies, incentives and subsidies implemented by the government to encourage the adoption of PV systems, they are expected to penetrate further into the energy distribution network in the near future (Pratik et al. 2025; Falama et al. 2023; Qusay Hassan 2021; Ortega-Arriaga et al. 2021). Several problems like voltage fluctuation, reverse power flow (Xie et al. 2024), stability issues (Zhang et al. 2023), harmonic and frequency disturbances (Oktoviano et al. 2020) arise due to integration of PV systems to the grid and gain greater attention as the PV system penetration exceeds 15% (Rajendran et al. 2025, Coddington et al. 2011). These PQ issues arise primarily from the intermittent nature of PV systems, along with various control mechanisms associated with the system (Salem et al. 2022). There are various PQ standards that specify limits for these variations (Kanchan et al. 2023).

Among the several PQ issues generated from grid integration of PV systems, interharmonics in grid current caused by MPPT control have drawn focus in the literature (Langella et al. 2016). Unlike harmonics, interharmonics occur at non-integer frequencies and are more challenging to filter. Interharmonics generated by the conventional MPPT methods arise from the periodic perturbations employed to reach maximum power. Perturb and Observe (P and O) algorithms have traditionally employed a constant perturbation. Larger perturbations enable faster tracking with higher oscillations around the MPP, leading to interharmonics, whereas a smaller step minimizes oscillations at the expense of slower tracking speed. The low-frequency power oscillations around the MPP caused by these perturbations are propagated to the dc link and cause interharmonics in the grid current (Sangwongwanich et al. 2018; V. Ravindran et al. 2020). Interharmonics can cause disturbances in different circuits, instruments and relays and resonance in various system components. Also, this may lead to tripping of

This is an open access article under the CC BY-NC-ND license (http://creativecommons.org/licenses/by-nc-nd/4.0/)

protection circuits, thereby unintentional disconnection of the PV system from the grid (Chicco et al. 2009). While most of the MPPT-related works focus on MPPT tracking speed and efficiency, the influence of MPPT parameters on PQ, especially interharmonic emission and its mitigation, has not been sufficiently investigated in the literature. To fill this research void, a Machine Learning (ML) based MPPT is proposed to mitigate interharmonics generated from MPPT control in a Grid Connected PV (GCPV) system. Unlike perturbation-based approach, the proposed model predicts the voltage corresponding to maximum power in each operating condition. The major research contributions in this work are given below:

i. Investigation of the influence of MPPT perturbation on interharmonic generation in a GCPV system.
ii. Development of a Gaussian Process Regression (GPR) based MPPT model for direct prediction of the maximum power PV operating voltage.
iii. Comparative evaluation of classical and ML-based MPPT techniques based on both tracking performance and PQ indices.
iv. Validation of the proposed approach for mitigating interharmonic distortion without compromising MPPT tracking accuracy.

In the subsequent content of this paper, a review of the literature is presented in the next section. Section 3 deals with the description of the system, and in Section 4, the effect of sampling frequency and perturbation step is described. Section 5 compares the performance of various MPPT strategies. The simulation findings are covered in section 6, while section 7 concludes the paper.

2. Literature Review

For alleviating the drawbacks of fixed perturbations in P and O algorithms, various adaptive step algorithms were proposed in the literature (Piegari et al. 2010; Kollimalla et al. 2014; Kandemir et al. 2017; Ibrahem et al. 2022). Although adaptive step algorithms perform better, they suffer from the limitations under rapidly varying irradiance conditions, like slow transient response, inability to track MPP accurately and higher complexity due to the real-time adaptation of perturbation step size. Recent advancements in data-driven intelligent techniques have enabled accurate prediction of the maximum power operating point using trained data, reducing reliance on complex PV mathematical models and enhancing MPPT performance under varying environmental conditions. Artificial Intelligence (AI) based MPPT methods offer faster tracking, accurate convergence and better efficiency compared to conventional methods (Mazumdar et al. 2024; Ukhsar et al. 2025). Among these, Artificial Neural Network (ANN) can predict operating point according to different inputs effectively, but it requires a large training dataset, leading to increased computational burden and controller implementation cost (Eyimaya, 2025; Padmanaban et al., 2022). Though a Fuzzy Logic Controller (FLC) can handle uncertainty, the derivation of fuzzy rules is difficult and time-consuming. However, the above two methods are not preferred for MPP tracking because of their ageing architecture and need for periodic tuning (Mostefa et al. 2017; Yap et al. 2020). Genetic Algorithms (GA) approach is mainly found suitable for optimization problems, yet they become computationally intensive as problem size grows (Peng et al. 2022; Kouro et al. 2015). Particle Swarm Optimization (PSO) has better adaptability to rapidly varying conditions and faster convergence with reduced computational burden. However, these techniques follow predefined update rules and parameters that need to be tuned again when there are significant changes in system characteristics (Ram et al. 2017; Lian et al. 2014). This drawback can be overcome by using ML models that are capable of adapting to new and unseen conditions once they are trained. They can be trained with the available manufacturer data to predict maximum power corresponding to each condition. Regression models effectively capture complex relationships between power and environmental conditions and then predict MPP accurately, which results in reduced interharmonic emission. By using regression learning for MPPT, PV systems can achieve higher efficiency, improved tracking speed and better performance under various operating conditions (Khanam et al. 2025; Nkambule et al. 2020).

Many ML-based MPPT works reported in the literature evaluate performance solely on the basis of prediction accuracy and tracking efficiency. This work explores the assessment of a GPR-based MPPT model from a performance as well as a power quality perspective.

3. GCPV System

Figure 1 presents the basic configuration of the GCPV system. In addition to MPPT control, control loops are incorporated to get constant DC-link voltage, grid synchronization, and inverter operation.

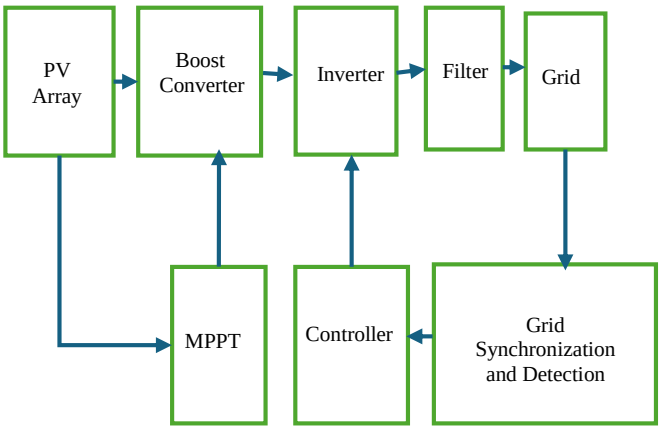


Fig. 1 GCPV system configuration

4. Mathematical Formulation of MPPT-Generated Interharmonics

MPPT is used for obtaining peak power from the PV array for different operating conditions. Because of its ease of use, P and O is the most used MPPT method. In this method, perturbations are applied to boost the converter duty cycle in each sampling interval.

The change in power and voltage is observed in adjacent sampling periods, and perturbations are applied in the desired direction till peak power is obtained. The perturbation magnitude and sampling frequency used significantly influence the magnitude and spectral location of interharmonics in the grid current. The set of equations describing the P&O algorithm is given in (1)-(6). The perturbation update rule is given by Equation (1). The decision rule for determining the sign in Equation (1) is given by Equations (2) to (4).

$$D_k = D_{k-1} \pm \Delta D \tag{1}$$

$$\Delta P = P_k - P_{k-1} \tag{2}$$

$$\Delta V = V_k - V_{k-1} \tag{3}$$

Where D_k and D_{k-1} are the duty cycles, P_k and P_{k-1} are PV powers, V_k and V_{k-1} are PV voltages at the k^{th} and $(k-1)^{th}$ sampling periods, and ΔD is the perturbation step.

$$\Delta D = \begin{cases} -\Delta D, if\ \frac{dp}{dv} > 0; \\ +\Delta D, if\ \frac{dp}{dv} < 0. \end{cases} \tag{4}$$

The condition for the MPP is shown by Equation (5).

$$\frac{dp}{dv} = 0 \tag{5}$$

The perturbation equations responsible for the oscillations around MPP in three adjacent sampling periods are given by (6).

$$D = \begin{cases} D_{MPP} + \Delta D;\ t_1 < t < (t_1 + T_s) \\ D_{MPP};\ (t_1 + T_s) < t < (t_1 + 2T_s) \\ D_{MPP} - \Delta D;\ (t_1 + 2T_s) < t < (t_1 + 3T_s) \end{cases} \tag{6}$$

Where D_{MPP} is the duty cycle near to MPP at time t_1, and T_s is the sampling period.

The PV voltage relations are obtained as given by Equation (7).

$$V_{PV} = V_{dc}(1 - D) \tag{7}$$

Where V_{PV} and V_{dc} are the voltage of the PV array and the voltage at dc link, respectively.

The change in PV voltage after a small perturbation of ΔD is given by (8),

$$\Delta V_{PV} = \pm V_{dc} \Delta D \tag{8}$$

The Taylor series expansion of PV power as a function of voltage around MPP can be truncated to 3 terms as in Equation (9),

$$P = P_{MPP} + \frac{dp}{dv}(V_{PV} - V_{MPP}) + \frac{1}{2}\frac{d^2p}{dv^2}(V_{PV} - V_{MPP})^2 \tag{9}$$

Where P_{MPP} is the maximum power and V_{MPP} is the voltage at maximum power.

At MPP, referring to Equation (5), the equation is simplified as in Equation (10) and can be expressed in terms of perturbation as in Equation (11),

$$P = P_{MPP} + \frac{1}{2}\frac{d^2p}{dv^2}(V_{PV} - V_{MPP})^2 \tag{10}$$

$$P = P_{MPP} \pm \frac{1}{2}\frac{d^2p}{dv^2}(V_{dc}\Delta D)^2 \tag{11}$$

Thus, it is clear that power oscillations are proportional to the square of the perturbation step size. Since MPPT is updated periodically after each sampling interval, the perturbation is not constant, and the power equation contains components of MPPT sampling frequency known as ripple power, as shown in Equations (12) and (13).

$$P(t) = P_{MPP} \pm \frac{1}{2}\frac{d^2p}{dv^2}(V_{dc}\Delta D)^2 sin^2\omega_m t \tag{12}$$

$$P(t) = P_{MPP} \pm \frac{1}{4}\frac{d^2p}{dv^2}(V_{dc}\Delta D)^2 \pm \frac{1}{4}\frac{d^2p}{dv^2}(V_{dc}\Delta D)^2 cos2\omega_m t \tag{13}$$

Where ω_m is the angular MPPT oscillation frequency, and the second and third terms in power form the ripple power.

These power oscillations modulate the amplitude of grid current and cause sideband components which are multiples of the MPPT oscillation frequency around the grid fundamental frequency and can be expressed as in Equation (14). The resulting grid current can be expressed as given by Equation (15).

$$f_{ih} = f \pm nf_m \tag{14}$$

$$i_g(t) = I_1 sin\omega t + I_{ih} sin(\omega \pm n\omega_m)t \quad (15)$$

Where f_{ih} is the interharmonic frequency and f_m is the MPPT oscillation frequency, n is an integer, ω is the angular grid frequency, I_1 and I_{ih} amplitude of the fundamental and interharmonic component of current.

From (13), it is clear that the ripple power component is responsible for interharmonics, and so the amplitude of interharmonics is proportional to ripple power, which is proportional to the square of perturbation size as given in Equation (16).

$$I_{ih} \alpha\ P_r \alpha\ (\Delta D)^2 \quad (16)$$

Thus, the changing MPPT sampling time shifts the location of prominent interharmonics, whereas the size of the MPPT perturbations influences the magnitude of interharmonics.

5. MPPT Control Strategies

The different MPPT approaches discussed in this work are the P and O algorithm using fixed perturbation, hybrid perturbation and a regression learner-based MPPT.

5.1. P and O Algorithm with Fixed Perturbation

In the P and O algorithm, the chosen size of perturbation has a significant effect on the efficiency, the time taken for tracking maximum power and interharmonics caused by MPPT control. A compromise is required between tracking speed and power quality while fixing the step size. The chosen step size may not be optimal in all operating conditions to track the exact MPP. This leads to energy loss and reduced efficiency.

5.2. Hybrid P and O Algorithm

The hybrid step approach with an adaptive step size near MPP and a fixed step for other operating points can improve the performance further.

Figure 2 displays the hybrid algorithm flowchart. The adaptive step size calculation used considers the variation in power in the adjacent sampling period, converter operating conditions and robustness against irradiance-dependent current variations. From PV and boost converter relations, the perturbation step size is given by Equation (17).

$$\Delta D = \frac{M * \Delta P}{I_{pv}^2 (1-D)} \quad (17)$$

Where ΔP is the change in PV array power in the two nearest sampling intervals, I_{pv} is the PV current, D is the duty cycle at which the boost converter was operated during the last sampling interval, M is a scaling factor, and ΔD is the perturbation employed in the duty cycle.

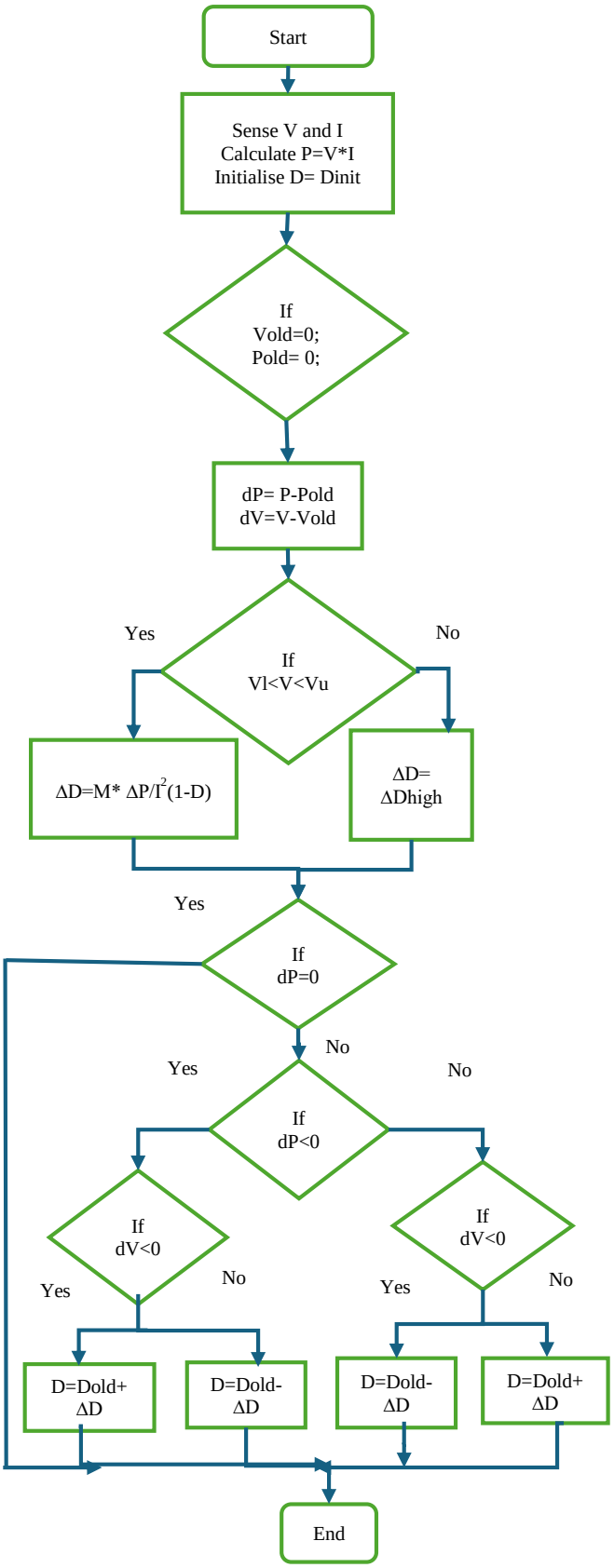


Fig. 2 Flowchart of Hybrid P and O

5.3. Regression based MPPT

The block diagram representation of different stages in the ML algorithm is given in Figure 3. The data required to train the model is prepared from the specifications of the PV array. Irradiance (G) and Temperature (T) are used as predictors while P_{mp} or V_{mp} forms the response for training the model with 80 percent of the data.

The model is then tested with the remaining 20 % of the dataset that the model has not seen in the training stage. This model is then used for MPPT control in the GCPV system.

The block diagram of ML-based MPPT control in the GCPV system is shown in Figure 4. The reference value predicted by the model is compared with the actual value, and a pulse is generated for the boost converter.

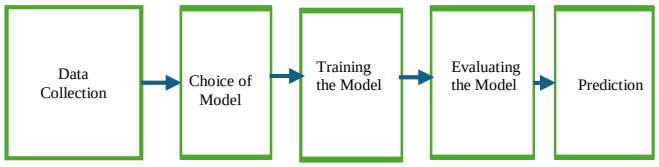


Fig. 3 Block diagram of ML algorithm

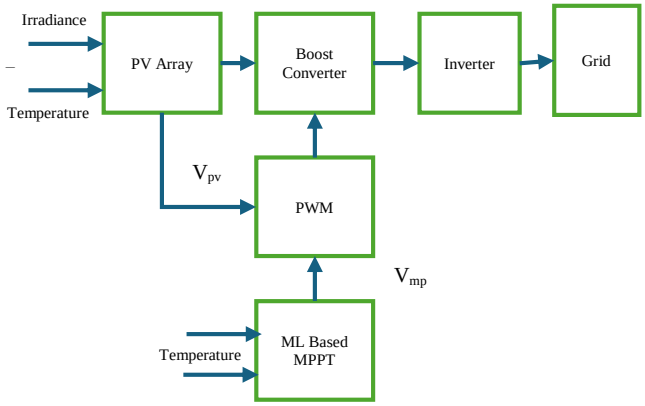


Fig. 4 Block diagram of ML-based MPPT

The regression model is trained using a data set of the system with G and T as input variables to predict MPP or voltage at MPP as the output variable. Then, the performance is evaluated using various error metrics.

Testing can be done with test data different from the trained data. The main error metrics used for comparing different models are given below with their equations from (18) to (20).

(i) Mean Absolute Error (MAE): It is the average of the error in the predicted and actual values.

$$MAE=\frac{1}{N}\sum_{k=1}^{N}|V(predicted,k)-V(actual,k)| \quad (18)$$

(ii) Mean Square Error (MSE): It is the average of the squares of error in the predicted and actual maximum values.

$$MSE=\frac{1}{N}\sum_{k=1}^{N}|V(predicted,k)-V(actual,k)|^2 \quad (19)$$

(iii) Root Mean Square Error (RMSE): It is the square root of the averaged squares of differences between predicted and actual maximum values.

$$RMSE=\sqrt{\frac{1}{N}\sum_{k=1}^{N}|V(predicted,k)-V(actual,k)|^2} \quad (20)$$

(iv) Coefficient of Determination (R^2): It indicates how well the prediction aligns with the actual value and lies in the range of 0 to 1. It shows the accuracy of the prediction by the model. Nearer the value is to 1, the better is the prediction.

$$R^2=\frac{\sum_{k=1}^{N}|V(predicted,k)-V(actual,k)|^2}{\sum_{k=1}^{N}|V(predicted,k)-V(actual,k)|^2} \quad (21)$$

where $V(predicted,k)$ is the predicted voltage corresponding to MPP and $V(actual,k)$ is the actual voltage for the given condition. All errors should be as low as possible, and the value of R^2 should be near to 1 for a best fit.

6. Simulation Results and Discussion

The 100 kW GCPV system model was implemented in the MATLAB/Simulink platform. The PV system is modeled using a PV array connected to a boost converter, followed by a DC-link and a three-phase inverter.

The sampling frequency is kept constant to ensure a consistent interharmonic frequency distribution for accurate comparison. DC link voltage control is achieved with a PI control loop. For synchronization with the grid, a Synchronous Reference Frame Phase-Locked Loop (SRF-PLL) is employed, and the inverter current is regulated using PI controllers in the dq reference frame.

The LCL filter is used at the inverter output to interface the system with the grid. The converter and control system were simulated using a fixed solver step size of 1 μs. The PI controllers and PLL were implemented in continuous time.

The same MPPT update rate and the same system parameters were used for both algorithms to ensure a consistent comparison. THD was evaluated from the steady-state grid-current waveform using an FFT analysis window spanning 10 cycles of the 50 Hz fundamental frequency. This corresponds to a frequency resolution of 5 Hz. The different simulation parameters employed are given in Table 1. The characteristic curves of the PV array used are shown in Figure 5.

Table 1. Simulation parameters

Parameter	Value
PV System power	100 kW at STC
Parallel strings	47
Modules in series	10
Switching frequency (Boost Converter)	5kHz
Inductance	1.45mH
Capacitance	3227µF
Inverter Switching Frequency	10 kHz
LCL filter	L=500 µH
	C=100 µF
DC link Controller	K_P= 0.25, K_i=300
Current Controller	K_p=10, K_i=20
MPPT	Perturbation Step Size of duty cycle = 0.001(high), 0.0001 (low)

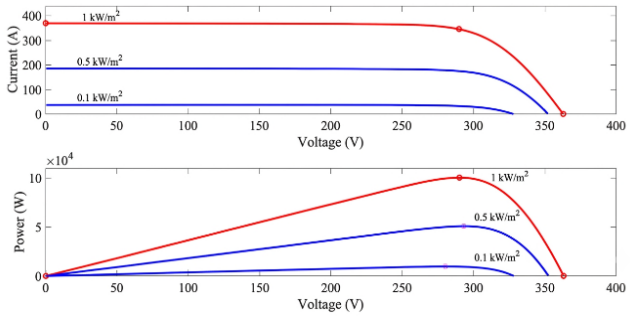


Fig. 5 Characteristic curves of PV array

MPPT control of the GCPV system was achieved using the P and O algorithm. The effect of irradiance on THD and interharmonic emission from the PV system is studied by FFT analysis in simulation for different irradiance at 25^{0}C. The amplitude spectrum at prominent harmonic and interharmonic frequencies between 50 Hz and 200 Hz is also studied.

The results are compared in Tables 2 and 3. The system has THD of 1.43% at Standard Test Condition (STC) of 1000W/m^2 irradiance, and 25^{o}C temperature, and THD is 6.78% at an irradiance of 200 W/m^2, which is not within acceptable limits.

The amplitudes of 80 Hz and 85 Hz components are less than 0.1% at STC, whereas at 200 W/m^2, it becomes 1.06% and 2.19%, respectively. The amplitude of the 250 Hz and 350 Hz components also increases with decreasing irradiance. Thus, the following insights can be drawn based on the study conducted.

(a) THD increases with decreasing irradiance.
(b) Lower irradiance values may lead to THD beyond standard limits even though the system has THD within acceptable limits (less than 5%) at STC.
(c) The amplitude of prominent interharmonic components is found to be increasing with decreasing irradiance.
(d) The amplitude of the dominant harmonic increases with decreasing irradiance values.

Table 2.THD for different irradiance at 25^{0}C

Irradiance(W/m^2)	1000	500	200
THD(%)	1.43	2.5	6.78

Table 3. Comparison of the amplitude of prominent frequency components

Frequency (Hz)	**Amplitude (%) 1000W/m^2**	**Amplitude (%) 500W/m^2**	**Amplitude (%) 200W/m^2**
75	0.03	0.26	0.41
80	0.05	0.38	1.06
85	0.02	0.09	2.19
175	0.06	0.22	0.5
180	0.05	0.43	0.45
190	0.03	0.09	0.53
250	1.06	1.81	4.33
350	0.5	1.03	2.64

The MPPT performance is analyzed at STC using fixed low, high and hybrid perturbations in the P and O algorithm, and the corresponding output power responses are illustrated in Figures 6, 7 and 8, respectively.

The results show that MPP tracking time for low step is 0.2 s, whereas 0.058 s with high step size and 0.08 s for the hybrid step P and O algorithm. Thus, it is evident that the hybrid perturbation approach offers a compromise between these two, achieving faster tracking than the low step size while maintaining reduced oscillations compared to the high step size.

Figures 9 and 10 represent the harmonic spectrum with low and high step sizes, respectively. The magnitude of interharmonic frequencies as well as THD increases with a high step size, even though it tracks MPP faster. Figure 11 shows the harmonic spectrum of the hybrid step P and O algorithm.

The measured THD values are 1.37% (low step), 1.43% (high step), and 1.38% (hybrid). The hybrid approach achieves fast tracking comparable to the high step size while maintaining THD levels close to the low step size, with reduced interharmonic amplitudes in the 50–200 Hz range.

For training the regression learner-based MPPT, data is extracted from Simulink PV array characteristics, which includes the Maximum Power (P_{mp}) and Voltage at Maximum Power (V_{mp}) Corresponding to Various Irradiance (G) and Temperature (T) conditions. A dataset consisting of 300 operating points was generated by varying the PV irradiance and temperature over the considered operating range.

The dataset includes the corresponding PV voltage, current, and voltage corresponding to maximum power values. Figures 12 and 13 give the contour plot of P_{mp} and V_{mp} over G and T, respectively. From these figures, it can be seen that. P_{mp} increases with irradiance and decreases slightly with temperature, whereas V_{mp} decreases with temperature and shows a relatively stable trend with increasing irradiance. Regression models capture the mapping between G, T, and PV outputs (P_{mp}, V_{mp}), enabling direct prediction after training. Using P_{mp} requires real-time power computation from voltage and current sensors, and it varies more sharply with irradiance than V_{mp}. Hence, models are developed to predict V_{mp} from G and T.

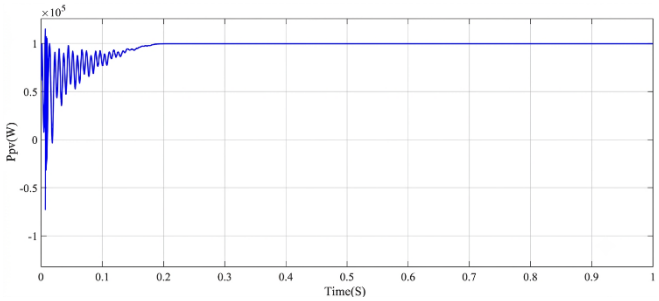


Fig. 6 Output power with low step P and O

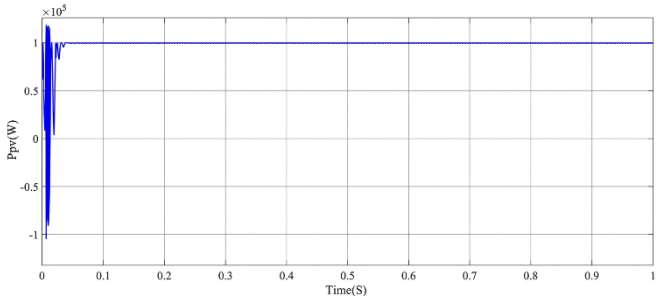


Fig.7 Output power with high step P and O

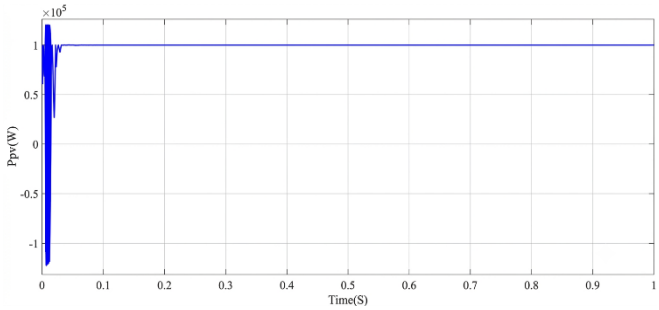


Fig. 8 Output power with hybrid step P and O

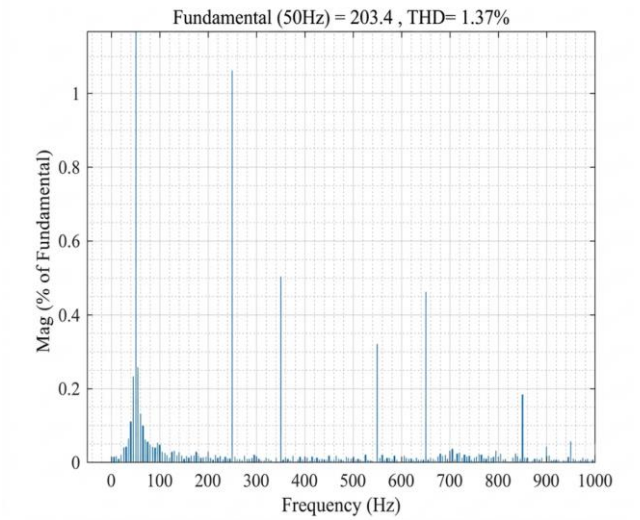


Fig. 9 Harmonic spectrum at STC with low step

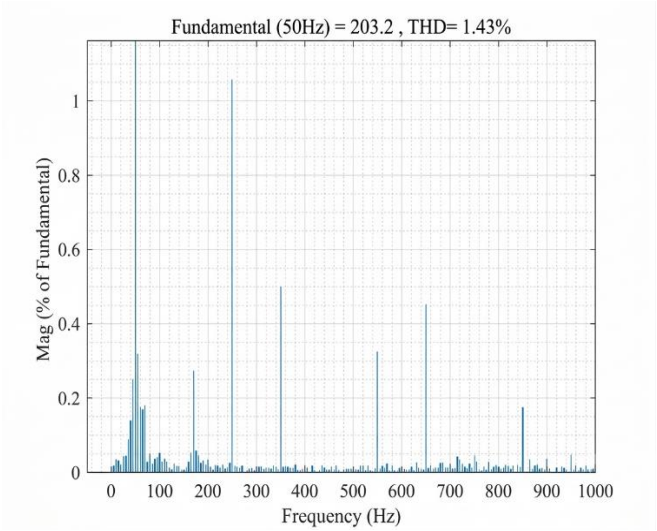


Fig. 10 Harmonic spectrum at STC with high step

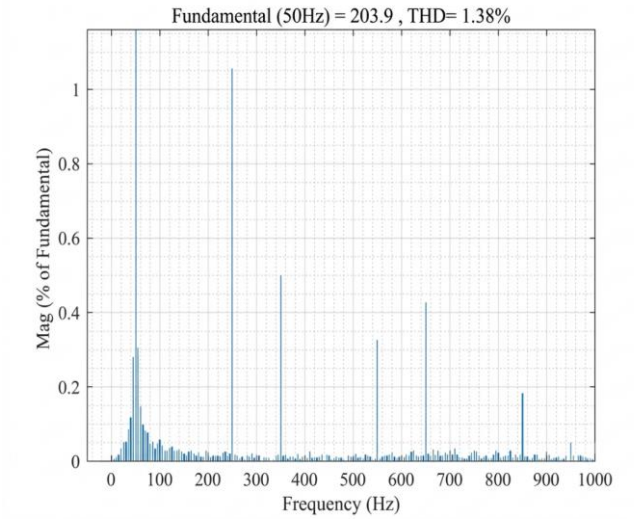


Fig.11 Harmonic spectrum at STC with hybrid step

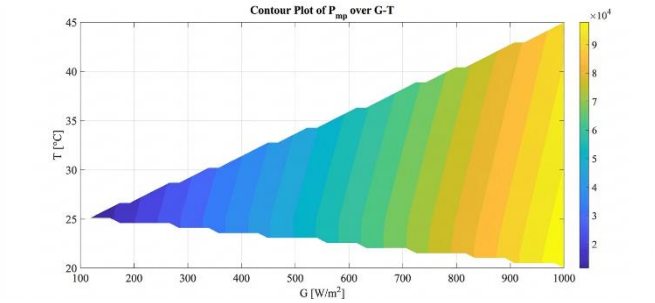


Fig. 12 Contour plot of P_{mp} over G-T

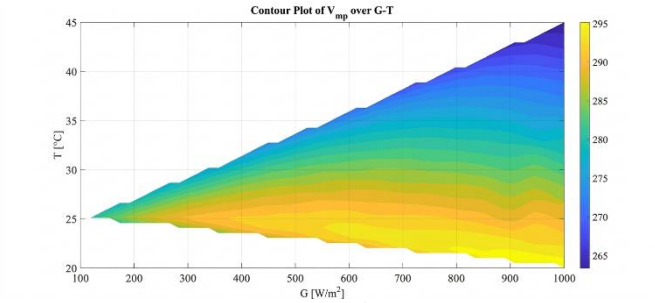


Fig. 13 Contour plot of V_{mp} over G-T

Table 4. Comparison of error metrics

Model	RMSE	MSE	MAE	R^2
Tree	1.72	2.99	1.22	0.95
SVM	0.89	0.79	0.58	0.98
ANN	0.82	0.67	0.5	0.98
GPR	0.64	0.41	0.32	0.99

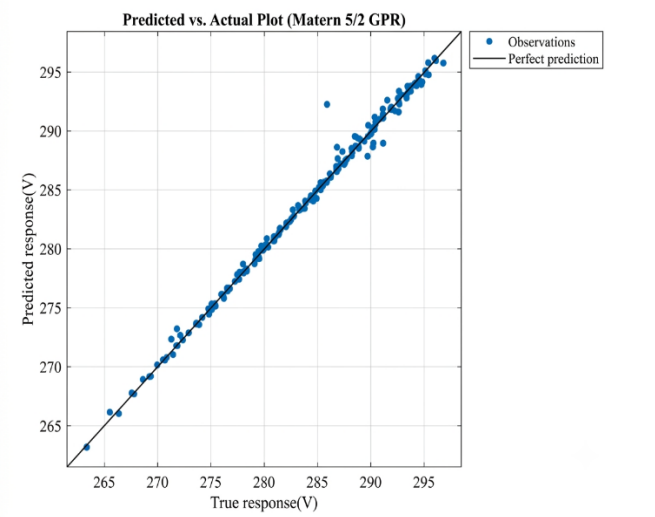


Fig. 14 Predicted vs actual plot

Table 4 compares error metrics of the selected models, showing that GPR achieves the lowest RMSE, MSE, and MAE, with the highest R^2. The Matérn 5/2 kernel was adopted to model the nonlinear PV characteristics, while the GPR hyperparameters were initialized with MATLAB default values and then fine-tuned based on prediction accuracy and MPPT performance. Figure 14 illustrates the predicted versus actual. V_{mp}, with most points closely aligned along the reference line.

GPR is a non-parametric regression that predicts outputs by modelling a distribution over possible functions instead of assuming a fixed model. Once trained with a set of G, T and corresponding V_{mp} values, GPR can predict V_{mp} for unseen conditions accurately.

The value predicted by GPR is compared with the actual PV voltage, and the duty cycle of the boost converter is changed accordingly. The predicted V_{mp} for 1000W/m^2 irradiance is given in Figure 15(a) and actual voltage of PV array V_{pv} in Figure 15(b). It is clear that V_{pv} follows predicted V_{mp}.

The MPPT tracking time is measured as the time taken to settle within (±2%) tolerance band of the corresponding maximum power following a change in operating conditions. The MPPT tracking efficiency is calculated as the ratio of the power extracted by the MPPT controller to the available maximum PV power, expressed as a percentage.

The output power curve in Figure 16 shows that output power is tracked fast in 0.01 s without any overshoot. The maximum output power of 100kW is obtained with an efficiency of 99.89% with zero overshoot.

The comparable results reported in literature are MPP rise time of 0.1558 s and efficiency greater than 94% obtained by support vector regression method with no overshoot (Mahesh et al.2023) and MPPT based on decision tree ML algorithm with response time of 0.16 s and efficiency greater than 93.93% (Mahesh et al.2022). Figure 17 shows the harmonic spectrum at 1000W/m^2 irradiance with a reduced THD of 1.35%. The magnitude of prominent interharmonic frequency components present in the P and O methods is reduced by the GPR model-based MPPT.

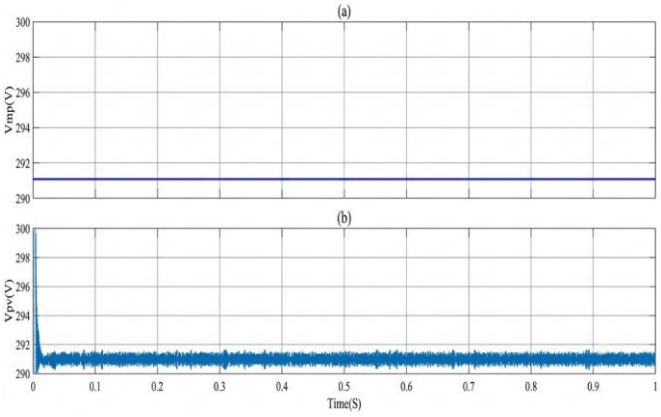


Fig 15 (a) V_{mp} predicted by GPR model, and (b) Actual PV array voltage at STC.

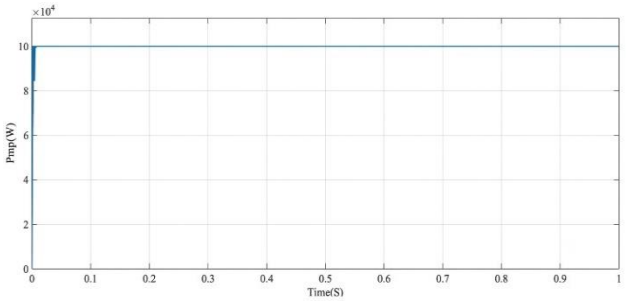


Fig. 16 Output power given by GPR MPPT at STC

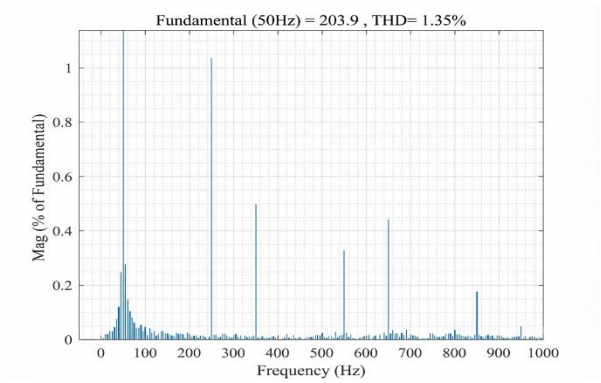


Fig. 17 Harmonic Spectrum of grid current at STC

The GPR and P&O algorithms were evaluated under identical irradiance, temperature, PV-array, converter, and simulation conditions to ensure a consistent comparison.

Table 5 compares THD, time taken to track maximum power and efficiency at STC of the four MPPT approaches. By using high perturbation in the algorithm, large oscillations around maximum power are produced, which reduces the efficiency of the algorithm.

Hybrid P and O show an improved performance with lesser MPP tracking time, reduced THD and good efficiency. GPR-based MPPT instantly tracks the maximum power accurately in 0.01 s with reduced THD and better efficiency. Total Interharmonic Distortion (TIHD) is determined from the FFT spectrum by calculating the root of the sum of squares of the interharmonic components and normalizing it with respect to the fundamental component.

Tables 6 and 7 show a comparison of THD, TIHD and interharmonics in each method for 200W/m^2, 25^{0}C. With GPR-based MPPT, THD as well as TIHD is reduced. Thus, it is clear that the regression learner-based method gives better tracking, efficiency and reduced PQ indices.

Table 5. Comparison of different MPPT algorithms at STC

MPPT Method	THD (%)	MPP tracking time(S)	Efficiency (%)
High Step P and O	1.43	0.058	99.62
Low Step P and O	1.37	0.2	99.68
Hybrid Step P and O	1.38	0.08	99.66
GPR-based MPPT	1.35	0.01	99.89

Table 6. Comparison of THD of different MPPT methods at 200 W/m^2 irradiance

MPPT	P and O MPPT			GPR-based MPPT
	High Step	Low Step	Hybrid Step	
THD (%)	6.78	5.48	6.14	5.4
TIHD(%)	3.84	0.88	2.82	0.67

Table 7. Comparison of prominent frequencies of different MPPT methods

Frequency (Hz)	Amplitude in % of the fundamental			
	Fixed High Step	Fixed Low Step	Hybrid Step	GPR-based MPPT
75	0.41	0.15	0.13	0.13
80	1.06	0.12	0.12	0.09
85	2.19	0.03	1.85	0.07
175	0.5	0.15	0.07	0.02
180	0.45	0.04	0.04	0.04
190	0.53	0.11	0.05	0.03

The simulation is repeated for a varying irradiance condition from 500W/m^2 to 800 W/m^2 at 25^{0}C. Figure 18(a) shows the change in irradiance, and Figure 18(b) shows that the model smoothly predicts V_{mp} corresponding to varying irradiance. The current and power of the PV array are shown in Figure 18(c) and Figure 18(d), respectively. It is clear that maximum power is tracked accurately with changes in irradiance conditions. Figure 19(a) shows the grid voltage, and Figure 19(b) shows the grid current, respectively, during the varying irradiance condition. The grid current amplitude increases as the irradiance increases.

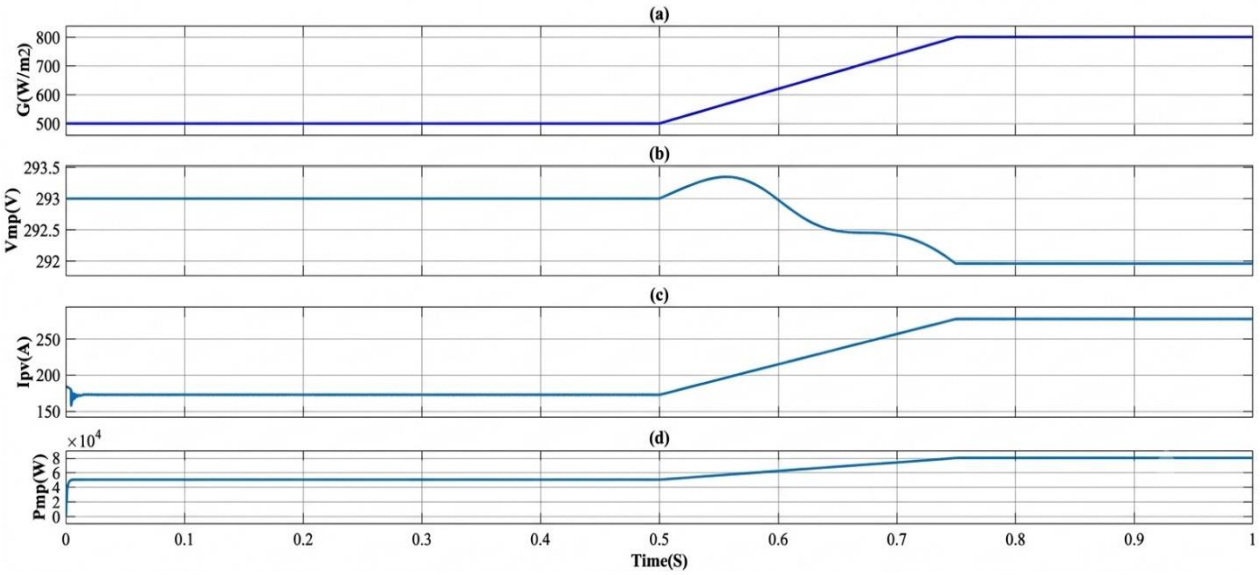


Fig. 18 (a) Varying irradiance, (b) V_{mp} predicted, (c) PV current, and (d) PV power.

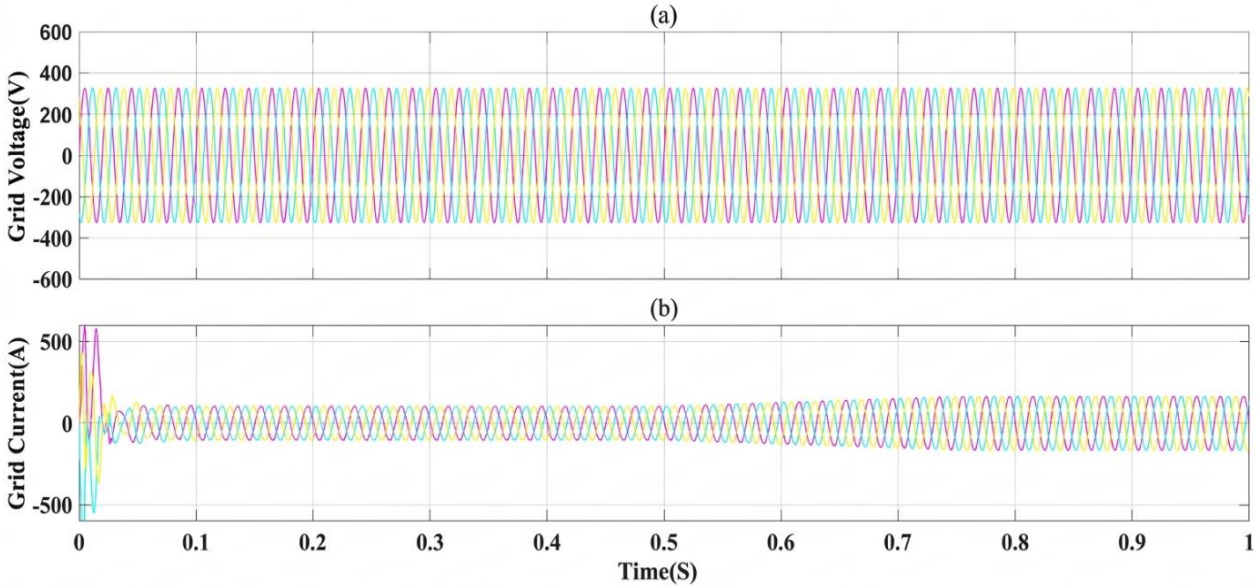


Fig. 19 (a) Grid voltage, and (b) Grid current under varying irradiance conditions.

7. Conclusion

This paper presents a Gaussian Process Regression based MPPT strategy for mitigating interharmonic emissions in grid-connected PV systems, particularly under low-power operating conditions.

The limitations of perturbation-based MPPT methods were analyzed by investigating the influence of perturbation step size on tracking performance and power quality. While larger perturbation steps improve tracking speed, they increase THD and TIHD, whereas hybrid P&O methods involve a performance trade-off. The proposed GPR-based MPPT predicts the optimum operating voltage from irradiance and temperature, eliminating steady-state perturbations and enabling smooth, accurate, and fast MPP tracking. Simulation results demonstrate that the proposed method achieves higher tracking performance with reduced overshoot while significantly lowering THD and TIHD compared with conventional perturbation-based approaches.

The present work is limited to simulation-based validation to confirm that GPR-based MPPT is a reliable and effective alternative to classical MPPT methods for GCPV applications with high penetration.

The practical feasibility of implementing the proposed GPR-based MPPT in real time is enhanced by performing the

computationally intensive GPR training process offline. During online operation, the controller only requires the acquisition of PV voltage and current measurements and the evaluation of the trained GPR model to estimate the MPP.

Acknowledgements

This work is supported by the Rashtriya Uchchatar Shiksha Abhiyan (RUSA Phase II) Major Project T4N, Proceedings No.37/2021/RUSA-SPD dated 27.04.2023.

Author Contributions

RR: Conceptualization, methodology, formal analysis, writing-original draft, PGL.; supervision, resources, project administration, RR, PGL.; writing- review and editing, project administration, validation. All authors have read and agreed to the published version of the manuscript.

Conflicts of Interest:

The authors declare no conflict of interest.

References

[1] Zakariya Sandi, "Examining Power Quality Challenges in Photovoltaic-Grid Integration: A Critical Review," *Journal of Power Energy and Control*, vol. 1, no. 1, pp. 12-23, 2024. [CrossRef] [Google Scholar] [Publisher Link]

[2] Pratik Joshi, Anand B. Rao, and Rangan Banerjee, "Review of Solar PV Deployment Trends, Policy Instruments, and Growth Projections in China, the United States, and India," *Renewable and Sustainable Energy Reviews*, vol. 213, pp. 1-17, 2025. [CrossRef] [Google Scholar] [Publisher Link]

[3] Ruben Zieba Falama et al., "A Comparative Analysis based Multi-Criteria Assessment of On/Off-Grid-Connected Renewable Energy Systems: A Case Study," *Energies*, vol. 16, no. 3, pp. 1-25, 2023. [CrossRef] [Google Scholar] [Publisher Link]

[4] Qusay Hassan, "Evaluation and Optimization of Off-Grid and On-Grid Photovoltaic Power System for Typical Household Electrification," *Renewable Energy*, vol. 164, pp. 375-390, 2021. [CrossRef] [Google Scholar] [Publisher Link]

[5] P. Ortega-Arriaga et al., "Grid Versus Off-Grid Electricity Access Options: A Review on the Economic and Environmental Impacts," *Renewable and Sustainable Energy Reviews*, vol. 143, pp. 1-17, 2021. [CrossRef] [Google Scholar] [Publisher Link]

[6] Yumeng Xie et al., "The Phenomenon and Suppression Strategy of Overvoltage caused by PV Power Reverse Flow," *Frontiers in Energy Research*, vol. 12, pp. 1-8, 2024. [CrossRef] [Google Scholar] [Publisher Link]

[7] Qianjin Zhang et al., "Voltage and Frequency Instability in Large PV Systems Connected to Weak Power Grid," *Frontiers in Energy Research*, vol. 11, pp. 1-12, 2023. [CrossRef] [Google Scholar] [Publisher Link]

[8] Oktoviano Gandhi et al., "Review of Power System Impacts at High PV Penetration Part I: Factors Limiting PV Penetration," *Solar Energy*, vol. 210, pp. 181-201, 2020. [CrossRef] [Google Scholar] [Publisher Link]

[9] Gowthamraj Rajendran, Reiko Raute, and Cedric Caruana, "Comprehensive Review of Solar PV Integration with Smart-Grids: Challenges, Standards, and Grid Codes," *Energies*, vol. 18, no. 9, pp. 1-80, 2025. [CrossRef] [Google Scholar] [Publisher Link]

[10] Michael H. Coddington et al., "Deploying High Penetration Photovoltaic Systems — A Case Study", *2011 37th IEEE Photovoltaic Specialists Conference*, Seattle, WA, USA, pp. 002594-002599, 2011. [CrossRef] [Google Scholar] [Publisher Link]

[11] W.A.A. Salem et al., "Grid Connected Photovoltaic System Impression on Power Quality of Low Voltage Distribution System," *Cogent Engineering*, vol. 9, no. 1, 2022. [CrossRef] [Google Scholar] [Publisher Link]

[12] Kanchan Jha, and Abdul Gafoor Shaik, "A Comprehensive Review of Power Quality Mitigation in the Scenario of Solar PV Integration into Utility Grid," *e-Prime - Advances in Electrical Engineering, Electronics and Energy*, vol. 3, pp. 1-18, 2023. [CrossRef] [Google Scholar] [Publisher Link]

[13] Roberto Langella et al., "On the Interharmonic Emission of PV Inverters under Different Operating Conditions," *2016 17th International Conference on Harmonics and Quality of Power (ICHQP)*, Horizonte, Brazil, pp. 733-738, 2016. [CrossRef] [Google Scholar] [Publisher Link]

[14] Ariya Sangwongwanich et al., "Analysis and Modeling of Interharmonics from Grid Connected Photovoltaic Systems," *IEEE Transactions on Power Electronics*, vol. 33, no. 10, pp. 8353-8364, 2018. [CrossRef] [Google Scholar] [Publisher Link]

[15] Vineetha Ravindran et al., "Time-Varying Interharmonics in Different Types of Grid-Tied PV Inverter Systems," *IEEE Transactions on Power Delivery*, vol. 35, no. 2, pp. 483-496, 2020. [CrossRef] [Google Scholar] [Publisher Link]

[16] Gianfranco Chicco, Jürgen Schlabbach, and Filippo Spertino, "Experimental Assessment of the Waveform Distortion in Grid Connected Photovoltaic Installations," *Solar Energy*, vol. 83, no. 7, pp. 1026-1039, 2009. [CrossRef] [Google Scholar] [Publisher Link]

[17] L. Piegari, and R. Rizzo, "Adaptive Perturb and Observe Algorithm for Photovoltaic Maximum Power Point Tracking," *IET Renewable Power Generation*, vol. 4, no. 4, pp. 317-328, 2010. [CrossRef] [Google Scholar] [Publisher Link]

[18] Ekrem Kandemir, Numan S. Cetin, and Selim Borekci, "A Comprehensive Overview of Maximum Power Extraction Methods for PV Systems," *Renewable. And Sustainable Energy Reviews*, vol. 78, pp. 93-112, 2010. [CrossRef] [Google Scholar] [Publisher Link]

[19] Sathish Kumar Kollimalla, and Mahesh Kumar Mishra, "A Novel Adaptive P&O MPPT Algorithm Considering Sudden Changes in the Irradiance," *IEEE Transactions on Energy Conversion*, vol. 29, no. 3, pp. 602-610, 2014. [CrossRef] [Google Scholar] [Publisher Link]

[20] Ibrahem Hussein, Özgür Çelik, and Ahmet Teke, "A Hybrid Random Parameters Modification to MPPT Algorithm to Mitigate Interharmonics from Single-Phase Grid Connected PV Systems," *Energy Reports*, vol. 8, pp. 6234-6244, 2022. [CrossRef] [Google Scholar] [Publisher Link]

[21] Debabrata Mazumdar et al., "Overview of Solar Photovoltaic MPPT Methods: A State of the Art on Conventional and Artificial Intelligence Control Techniques," *International Transactions on Electrical Energy Systems*, vol. 2024, no. 1, pp. 1-24, 2024. [CrossRef] [Google Scholar] [Publisher Link]

[22] Ukhsar, Aidha Muhammad Ajmal, and Yongheng Yang, "Global Maximum Power Point Tracking of Photovoltaic Systems using Artificial Intelligence," *Energies*, vol. 18, no. 12, pp. 1-27, 2025. [CrossRef] [Google Scholar] [Publisher Link]

[23] Süleyman Emre Eyimaya, "Efficiency Analysis of Artificial Intelligence and Conventional Maximum Power Point Tracking Methods in Photovoltaic Systems," *Applied Sciences*, vol. 15, no. 10, pp. 1-20, 2025. [CrossRef] [Google Scholar] [Publisher Link]

[24] K. Padmanaban, A. Shunmugalatha, and M.S. Kamalesh, "Design and of a New, Fast and Efficient MPPT Controller under Different Solar Irradiance Conditions," *International Journal of Photoenergy*, vol. 2022, no. 1, pp. 1-15, 2022. [CrossRef] [Google Scholar] [Publisher Link]

[25] Mostefa Kermadi, and El Madjid Berkouk, "Artificial Intelligence-based Maximum Power Point Tracking Controllers for Photovoltaic Systems: Comparative Study," *Renewable and Sustainable Energy Reviews*, vol. 69, pp. 369-386, 2017. [CrossRef] [Google Scholar] [Publisher Link]

[26] Kah Yung Yap, Charles R. Sarimuthu, and Joanne Mun-Yee Lim, "Artificial Intelligence based MPPT Techniques for Solar Power System: A Review," *Journal of Modern Power Systems and Clean Energy*, vol. 8, no. 6, pp. 1043-1059, 2020. [CrossRef] [Google Scholar] [Publisher Link]

[27] Dan Peng, Zhanpeng Xu, and Peijian Xu, "Research on MPPT Simulation of Photovoltaic Power Generation based on Improved Genetic Algorithm," *2022 International Conference on Artificial Intelligence of Things and Crowdsensing (AIoTCs)*, Nicosia, Cyprus, pp. 493-497, 2022. [CrossRef] [Google Scholar] [Publisher Link]

[28] Samir Kouro et al., "Grid-Connected Photovoltaic Systems: An Overview of Recent Research and Emerging PV Converter Technology," *IEEE Industrial Electronics Magazine*, vol. 9, no. 1, pp. 47-61, 2015. [CrossRef] [Google Scholar] [Publisher Link]

[29] J. Prasanth Ram, T. Sudhakar Babu, and N. Rajasekar, "A Comprehensive Review on Solar PV Maximum Power Point Tracking Techniques," *Renewable and Sustainable Energy Reviews*, vol. 67, pp. 826-847, 2017. [CrossRef] [Google Scholar] [Publisher Link]

[30] Kuo-Lung Lian, J.H. Jhang, and I.S. Tian, "A Maximum Power Point Tracking Method based on Perturb-and-Observe Combined with Particle Swarm Optimization," *IEEE Journal of Photovoltaics*, vol. 4, no. 2, pp. 626-633, 2014. [CrossRef] [Google Scholar] [Publisher Link]

[31] Jobeda J. Khanam et al., "Machine Learning-Driven MPPT Techniques for Optimal Solar Energy Utilization," *SoutheastCon*, Concord, NC, USA, pp. 309-313, 2025. [CrossRef] [Google Scholar] [Publisher Link]

[32] Mpho Sam Nkambule et al., "Comprehensive Evaluation of Machine Learning MPPT Algorithms for a PV System under Different Weather Conditions," *Journal of Electrical Engineering and Technology*, vol. 16, no. 1, pp. 411-427, 2020. [CrossRef] [Google Scholar] [Publisher Link]

[33] P. Venkata Mahesh, S. Meyyappan, and RamaKoteswaraRao Alla, "Support Vector Regression Machine Learning based Maximum Power Point Tracking for Solar Photovoltaic systems," *International Journal of Electrical and Computer Engineering Systems*, vol. 14, no. 1, pp. 100-108, 2023. [CrossRef] [Google Scholar] [Publisher Link]

[34] P. Venkata Mahesh, S. Meyyappan, and RamaKoteswaraRao Alla, "Maximum Power Point Tracking using Decision-Tree Machine-Learning Algorithm for Photovoltaic Systems," *Clean Energy*, vol. 6, no. 5, pp. 762-775, 2022. [CrossRef] [Google Scholar] [Publisher Link]